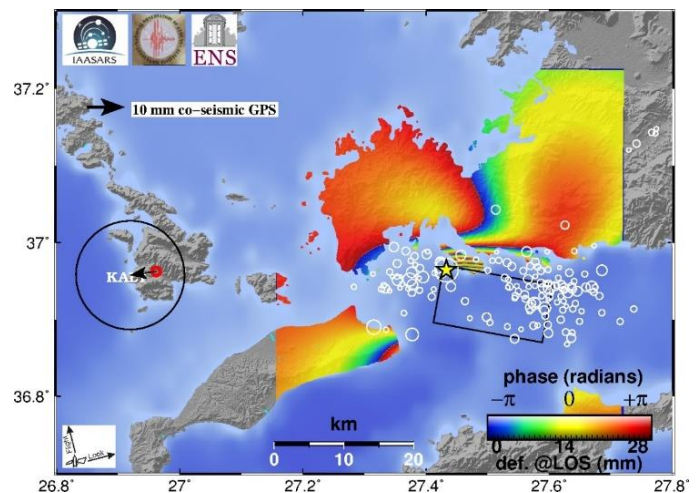


**Co-seismic  
deformation and  
preliminary fault  
model of the July  
20, 2017 M6.6 Kos  
earthquake,  
Aegean Sea**

30 JULY  
2017

**A. Ganas, P. Elias,  
S. Valkaniotis, P.  
Briole, V.  
Kapetanidis, I.  
Kassaras, A.  
Barberopoulou, P.  
Argyrakis, G.  
Chouliaras, A.  
Moshou**



# Co-seismic deformation and preliminary fault model of the July 20, 2017 M6.6 Kos earthquake, Aegean Sea<sup>1</sup>

**Athanassios Ganas<sup>1</sup>, Panagiotis Elias<sup>2</sup>, Sotirios Valkaniotis<sup>3</sup>, Pierre Briole<sup>4</sup>  
Vasilios Kapetanidis<sup>5</sup> Ioannis Kassaras<sup>5</sup> Aggeliki Barberopoulou<sup>6</sup>,  
Panagiotis Argyrakis<sup>1</sup>, Gerassimos Chouliaras<sup>1</sup> and Alexandra Moshou<sup>1</sup>**

<sup>1</sup>National Observatory of Athens, Institute of Geodynamics, Lofos Nymfon, Thission, 11810 Athens, Greece, [aganas@noa.gr](mailto:aganas@noa.gr) [pargyrak@noa.gr](mailto:pargyrak@noa.gr) [g.choul@noa.gr](mailto:g.choul@noa.gr) [amoshou@noa.gr](mailto:amoshou@noa.gr)

<sup>2</sup>National Observatory of Athens, Institute of Astronomy, Astrophysics, Space Applications and Remote Sensing, Vas. Pavlou & I. Metaxa, GR-15 236 Penteli, Greece [pelias@noa.gr](mailto:pelias@noa.gr)

<sup>3</sup>Koronidos Str., 42131, Trikala, Greece [valkaniotis@yahoo.com](mailto:valkaniotis@yahoo.com)

<sup>4</sup>Ecole Normale Supérieure, PSL research University, Laboratoire de Géologie - UMR CNRS 8538, Paris, France [briole@ens.fr](mailto:briole@ens.fr)

<sup>5</sup>National and Kapodistrian University of Athens, Faculty of Geology and Geoenvironment, University Campus- Zografou, Athens GR 157 84, Greece [vkapetan@geol.uoa.gr](mailto:vkapetan@geol.uoa.gr) [kassaras@geol.uoa.gr](mailto:kassaras@geol.uoa.gr)

<sup>6</sup>AIR Worldwide, 131 Dartmouth St., Boston MA USA [aggeliki.barberopoulou@gmail.com](mailto:aggeliki.barberopoulou@gmail.com)

## Summary

We present a preliminary fault model from inversion of geodetic data regarding the shallow earthquake (M6.6) on July 20, 2017 between Kos (Greece) and Bodrum (Turkey). The model is constrained by geodetic data from Sentinel 1A/B interferograms, processed by SNAP software. The best-fit model favors a 40° north-dipping normal fault in agreement with published MT solutions for this event, that suggest pure normal faulting in a E-W direction. The fault is located offshore. Surface deformation reached about 20 cm onshore islet Karaada.

---

<sup>1</sup> This report was released to EMSC on July 30, 2017 12:20 UTC

## 1. Introduction

On July 20, 2017 22:31 UTC (01:31 local time) a strong, shallow earthquake occurred offshore the island of Kos, SE Aegean Sea (NOA magnitude Mw6.6, USGS Mw6.6). The earthquake registered VI-VII instrumental intensities<sup>2</sup>, and caused severe damage to the building stock of Kos <http://www.telegraph.co.uk/news/2017/07/20/large-earthquake-reported-turkish-coast-greek-island-kos/> including partial collapses that killed two people and seriously injured several others. Among the secondary effects it is worthy to mention a) soil spreading that caused damage of the port of the town of Kos and b) a local tsunami that flooded the town of Bodrum (Fig. 1) and vicinity. No extensive landsliding was reported from either Greece or Turkey and preliminary investigation by S. Valkaniotis of Sentinel 2A/B imagery (July 22 and 24 acquisitions) showed no landslide scars.

The M6.6 epicentre was determined near the uninhabited islet of Karaada (Fig. 1; offshore Bodrum, SW Turkey) by the main seismic networks in the region: NOA at 36.9643°North 27.4332°East, by EMSC at 36.96°N 27.45°E, and by KOERI 36.9620°N and 27.40535°E. The focal parameters of the mainshock indicate nearly E-W strike and moderate dip angles; they are summarised in Table 1. The mainshock occurred in a region of predominantly extensional tectonics as evidenced by the formation of Quaternary marine grabens, namely the NE-SW Kos graben (Tibaldi et al., 2008; Nomikou et al., 2011; 2013) and the east-west trending Gökova grabens (Ulug et al. 2005, Tur et al., 2015; Fig. 1). Crustal deformation is oriented mainly N-S ( $\pm 20^\circ$ ) based on orientation of GPS extension axis (Kreemer and Chamot-Rooke, 2004; Floyd et al., 2010) as well as on seismic tension axes (i.e. principal stress components deduced from earthquake focal mechanisms; Kiratzi and Louvari, 2003; Irmak, 2013; Yolsal-Çevikbilen et al., 2014). A 4 mm/yr extension rate has been proposed by Vernant et al., (2014) across the Gulf of Gökova (Kerameikos). However, some strike-slip tectonics is also expected in this region because of the interaction of the Aegean microplate with the down-going Nubia plate (Ganas and Parsons, 2009, their Fig. 6). Recent offshore seismic data provide evidence for young strike-slip motions (Iscan et al, 2013).

---

<sup>2</sup> <https://shake.gein.noa.gr/sm/noa2017odde/intensity.html>

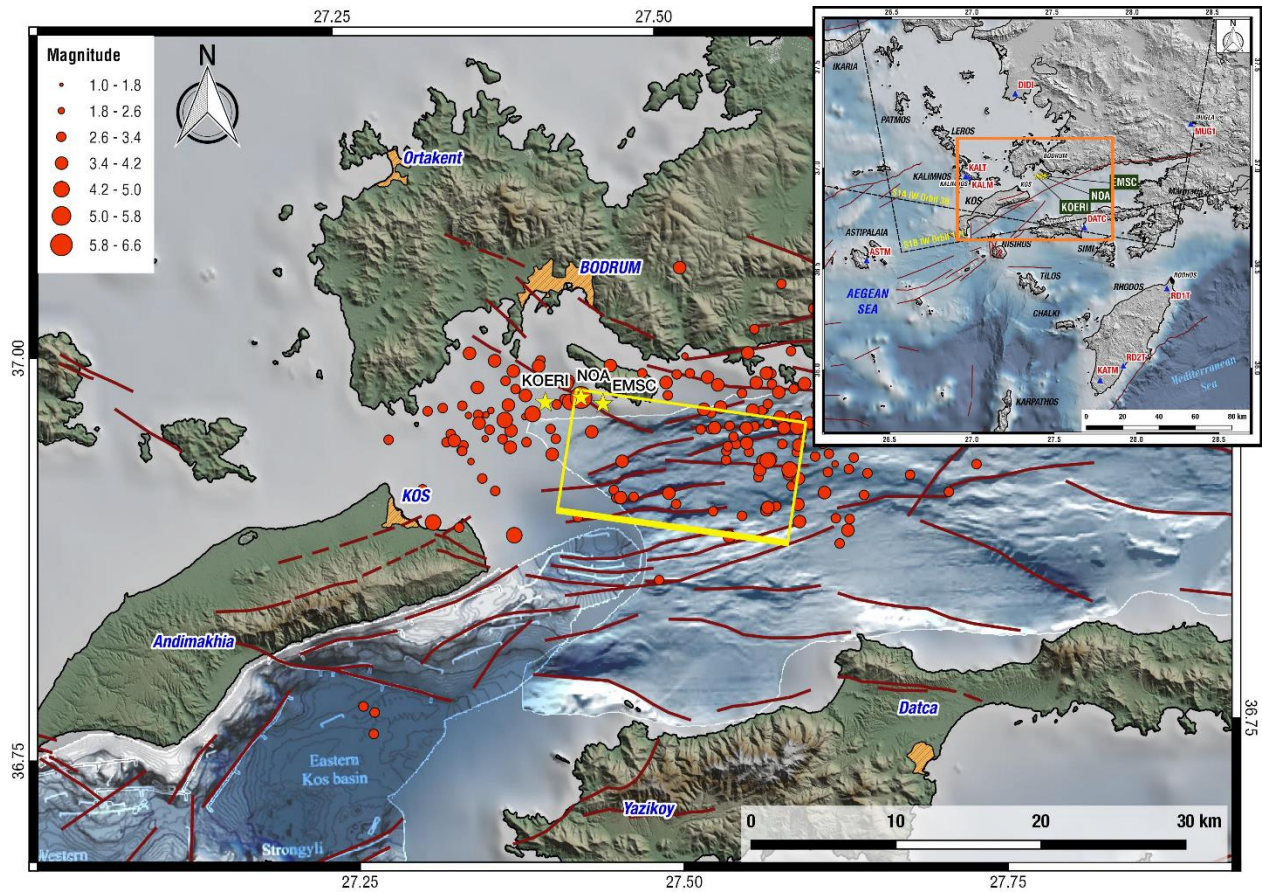


**Figure 1** Location map and relief model of the region affected by the Kos earthquake (20/7/2017 22:31 UTC; M6.6). Yellow stars denote epicentre determinations of mainshock by NOA, KOERI and EMSC. Red lines are active faults from various sources including Ganas et al., (2013), Nomikou et al., (2013) and Tur et al., (2015). Red circles are NOA aftershock epicentres (revised locations as of 29/7/2017 09:50 UTC; circle size is proportional to local magnitude). Yellow rectangle indicates surface projection of the north-dipping seismic fault determined by SAR interferometry (thicker line denotes upper edge). Land elevation from ALOS GSDM, bathymetry from EMODNET, Nomikou (2004) and İşcan et al. (2013). Inset box at upper right shows location within South Aegean Sea, as well as Sentinel frames (black boxes; only part of the 250 km frame is shown) and GNSS permanent stations (blue triangles).

**Table 1.** Moment tensor solutions for the mainshock reported at the EMSC web-site by various institutions. These focal mechanisms are computed using methods that attempt to find the best fit to the waveforms of seismic waves observed at each station.

Institute	Mw	M <sub>0</sub> (dyn*cm)	Depth (km)	Strike (°)	Dip (°)	Rake (°)	Strike (°)	Dip (°)	Rake (°)
GCMT	6.6	9.70E+25	12	275	36	-85	89	54	-94
CPPT	6.7	1.42E+26	10	290	26	-58	76	68	-104
IPGP	6.6	9.70E+25	9	284	32	-71	82	60	-102
GFZ	6.6	9.70E+25	11	98	35	-82	270	56	-94
USGS	6.6	1.13E+26	11.5	281	34	-78	87	56	-97
KOERI	6.6	1.13E+26	6	286	53	-72	78	40	-112
INGV	6.7	1.3E+26	11.3	296	49	-55	68	52	-124
NOA	6.6	8.93E+25	6	265	43	-102	102	48	-79
AUTH	6.5	8.93E+25	7	93	49	-91	275	41	-88
NKUA	6.6	8.89E+25	11	267	38	-110	112	55	-75

## 2. Geodetic Data and Methods

### 2.1 INSAR data processing

Regarding InSAR processing we used Sentinel 1A/1B satellite data (C-band; one fringe corresponds to half wavelength or 28 mm). In this study for interferometric processing, both ascending track 131 and descending track 36 Sentinel-1A IW swath mode SLC images covering the pre- and post- Kos 2017 seismic event period were downloaded from ESA's Sentinel Hub site. Four pairs of ascending and two descending co-seismic, as well as one descending pre-seismic interferograms have been created. Each interferogram provides an estimation of the relative motion of the earth surface in the viewing direction of the satellite (LOS); the direction is different for ascending and descending tracks (Fig. 2top, bottom). SAR data processing was performed using ESA's SNAP software. After selecting the appropriate sub-swaths containing Kos and surrounding area the co-registration step was carried out such as the pixel of the slave images to be moved to align with pixels of the master at a sub-pixel accuracy. Then a shift by a small amount in azimuth and range direction was performed on the slave bands. Based on preliminary orbital information,

the orbital contribution was estimated and subtracted from the complex interferograms. The interferograms were flattened by removing the topographic phase based on a reference DEM (~90m) extracted from SRTM. In order to increase the noise to signal ratio a power spectrum filter (Goldstein & Werner 1998) was applied to reduce the effects of phase noise while multilooking operation was applied using a factor of 24:6 (azimuth: range) in order to reduce the standard deviation of the noise level and obtain approximately square pixel. The comparison of the processed interferograms show that the fringe pattern deformation appears to all co-seismic interferograms, meaning that it is related to co-seismic deformation and not related to atmospheric induced phase as appear to both ascending and descending interferometric pairs.

Finally, two co-seismic interferograms were selected in ascending and descending geometry of acquisition characterized by low spatial and temporal geometrical baselines. The interferograms are of good quality and contain the phase difference produced by the main event. Although the two interferograms are similar, they are not identical due to the different acquisition geometry (Figure 2). Areas characterized by low coherence, the noisy areas in the images, can be attributed to temporal decorrelation mainly due to the vegetation land cover areas that exist on the island and atmospheric effects. Relatively low magnitude aftershocks (up to  $M_L 4.8$ ; NOA magnitudes) happened in the period covered partially by both pairs; they did not affect the deformation signal as all those events occurred offshore and with moderate magnitudes. The surface deformation, formed by 7.5 fringes (ascending orbit) and 6 fringes (descending), occurs onshore the island Karaada (offshore Bodrum, Fig. 1, Fig. 2) close to where the main event epicenter is located. The maximum value of deformation reached in the line-of-sight (LOS), is 20 cm away from the satellite both in descending and ascending interferograms, i.e. the co-seismic ground motion at Karaada was subsidence. The deformation that occurred in the area between the two islands (Kos and Karaada) could not be measured, being off-shore, but can be estimated through modelling.

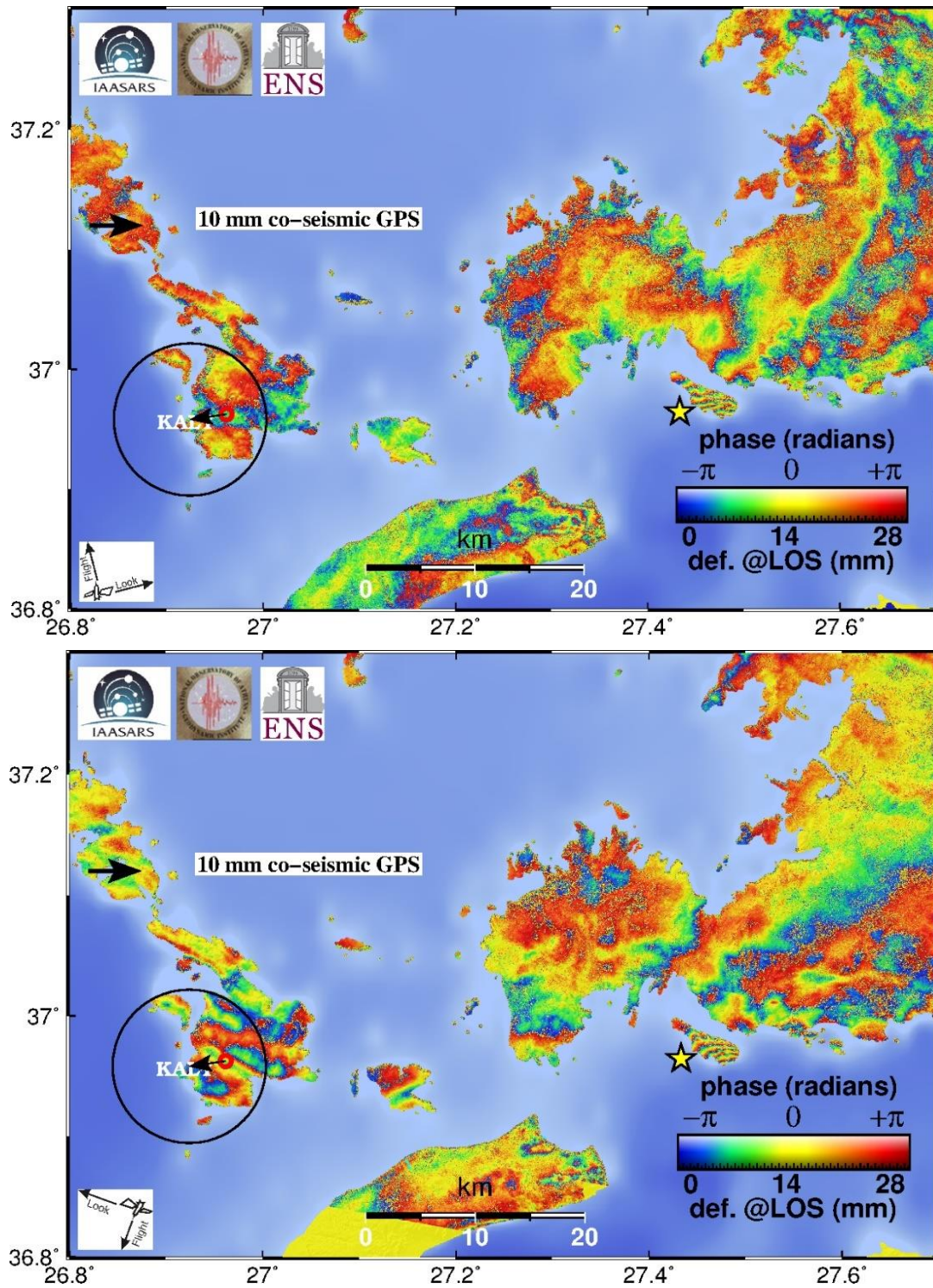


Figure 2. Sentinel 1A wrapped interferogram ascending orbit (a) descending orbit (b). Yellow star indicates the earthquake epicentre (NOA revised location; <http://bbnet.gein.noa.gr>)

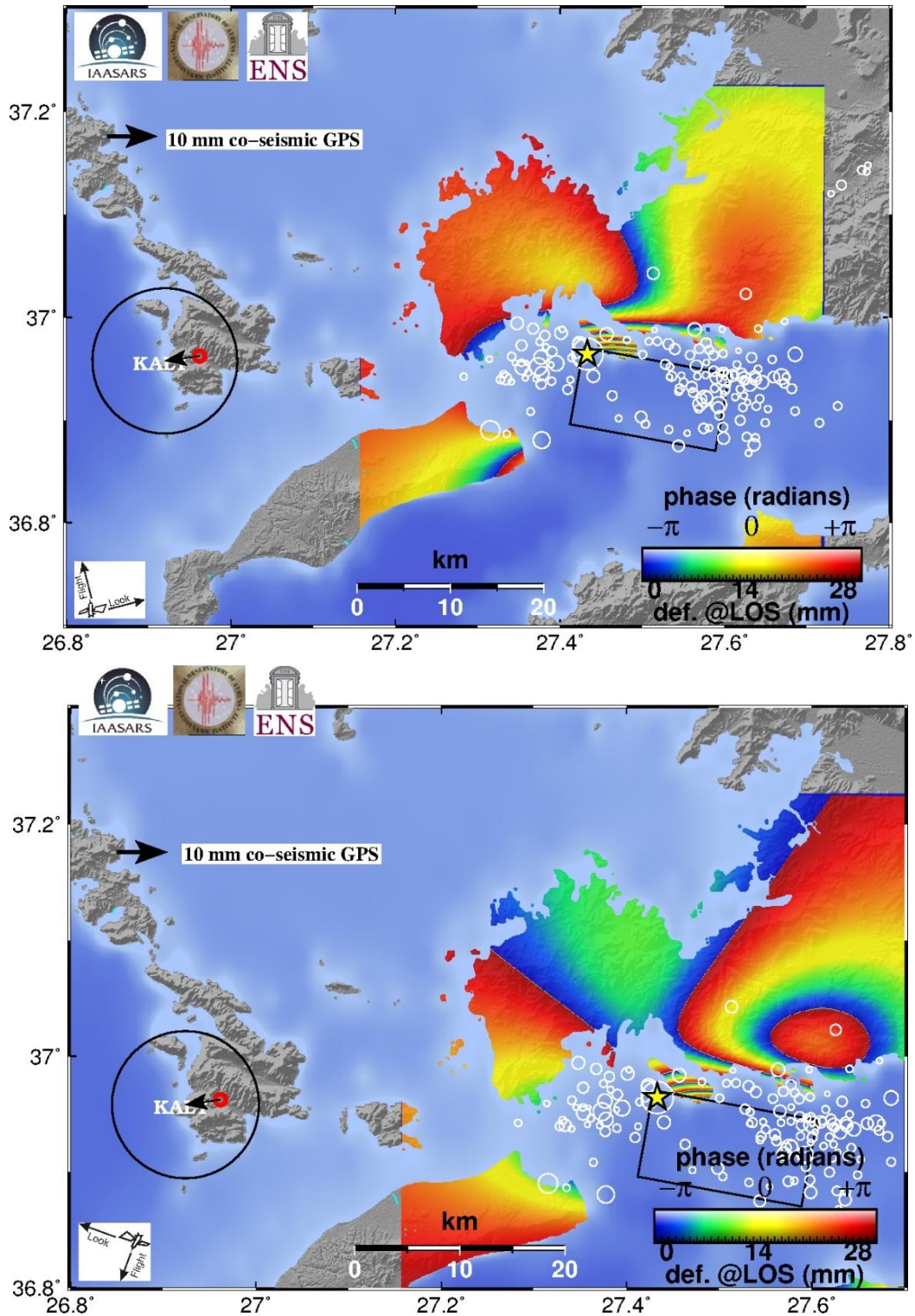


Figure 3 Co-seismic fault models (top, bottom), for ascending and descending orbits, respectively. The inferred source for the mainshock is shown by the black rectangle (surface projection). Yellow star indicates the earthquake epicentre (NOA revised location; <http://bbnet.gein.noa.gr>).

## 2.2 GNSS offsets

We analysed GNSS data (1-s and 30-s observations) in order to detect co-seismic offsets in position time series. The data originate from several networks in Greece (METRICANET, URANUS and NOANET) and one network in Turkey and were released on July 25, 2017<sup>34</sup>. Due to the size of the earthquake and its offshore location we expect small (mm-size) offsets at station locations as seen in Fig. 1 (blue triangles; minimum distance to NOA epicentre is 33 km).

A preliminary calculation of expected GNSS offsets using the fault model presented in Fig 1 (yellow rectangle) indicated that perhaps station DATC (Datsa, Turkey) could have recorded the earthquake. This station is equipped with a dual frequency receiver and geodetic antenna and its data was processed in kinematic Precise Point Positioning (PPP) mode (Fig. 4). The co-seismic offsets are clearly visible in the North-South horizontal component (about 3 cm towards South; Fig. 4 top line) and in the East-West component (about 1 cm towards East; Fig. 4 middle line). No seismic signal is visible in the Up component (Fig. 4, bottom line).

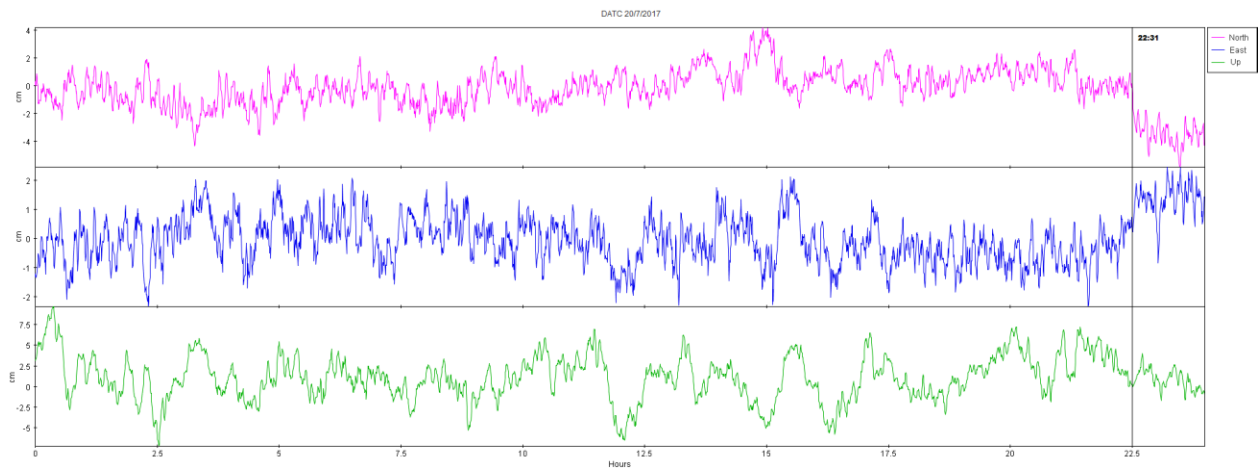


Figure 4. Graph showing North, East, Up Displacements of GNSS station DATC (Latitude: N 36° 42' 30.86228", Longitude :E 27° 41' 30.60475", Height: 59.176 m) due to seismic waves from the 20/7/2017 M6.6 Earthquake. The high rate data were analyzed with GIPSY/OASIS (<https://gipsy-oasis.jpl.nasa.gov/>) applying PPP Kinematic positioning, with the use of JPL Rapid Orbits/Clocks. Horizontal axis is hours, vertical axis is displacement (cm). Thin vertical line near 22.5 hrs indicates time of earthquake. Processing by P. Argyrakis (NOA).

<sup>3</sup> [http://www.gein.noa.gr/services/GPSData/1\\_test/kos/](http://www.gein.noa.gr/services/GPSData/1_test/kos/)

<sup>4</sup> GCM (Turkey) also opened 1s data of CORS sites in the region <https://www.hgk.msb.gov.tr/haber-237-gokova-korfezi-depremi-cevresindeki-tusaga-aktif-istasyonlarina-ait-veriler.html>

## 2.3 Fault Inversion

To do the inversion we picked samples of surface displacement every 400-500 m along every fringe in both ascending and descending pass interferograms considering the LOS unit vectors. Following the procedure by Briole et al., (1986) and using one of the nodal planes suggested by seismology as starting point (Table 1; USGS north-dipping plane is  $285^{\circ}/39^{\circ}/-73^{\circ}$ ) we tried several inversions by a) locking the strike and dip to  $N280^{\circ}E$  and  $40^{\circ}$  respectively, b) increasing the fault width to 11 km, c) using an a priori length of 16 km (half-length 8 km), d) keeping the fault upper edge fixed at 1 km depth (and modify later if needed), and inverting for the two following parameters: i) map (horizontal-plane) coordinates of the centre of the fault upper-edge ii) amount of slip (assuming pure normal faulting). In this way, we obtained a seismic moment of  $M_0 = 10^{19}$  Nm, which is very close to seismologically determined moments (NOA  $8.9 \times 10^{18}$  N-m; USGS  $1.1 \times 10^{19}$  N-m) and thus the co-seismic slip should be of the order of 1.5 m.

Compared to similar magnitude events the source time function is a bit short<sup>5</sup> (showing a main triangular pulse with a duration of 5s), so it is expected a) a fault size not very big and b) a slip amount larger than average. We also tried with a fixed amount of slip and inverted for the two map coordinates of the centre of the fault upper-edge only in order to constrain it better due to the limited number of picked fringes (see Fig. 2). The results did not vary much so we consider our solution as stable. Our preferred solution is summarized in the Table 2 below. A vertical cross section depicting the model fault plane is shown in Fig. 5. The fault upper-edge is projected to the sea-bottom near the Gulf of Gokova western ridge (Figure 1; Tur et al, 2015, their figure 3).

**Table 2.** Parameters of the 20/7/2017 seismic fault determined from inversion of geodetic data

<b>Seismic Fault Parameter</b>	<b>Value</b>
Fault length (km)	16
Fault width (km)	11
Fault Dip angle (degrees)	40
Azimuth (clockwise from North – degrees)	280
Fault Slip – normal (m)	1.5
Centre of upper edge of the fault (UTM35 East, North)	544600, 4082000
Top of the fault (km)	1

<sup>5</sup> <http://geoscope.ipgp.fr/index.php/en/catalog/earthquake-description?seis=us20009ynd>

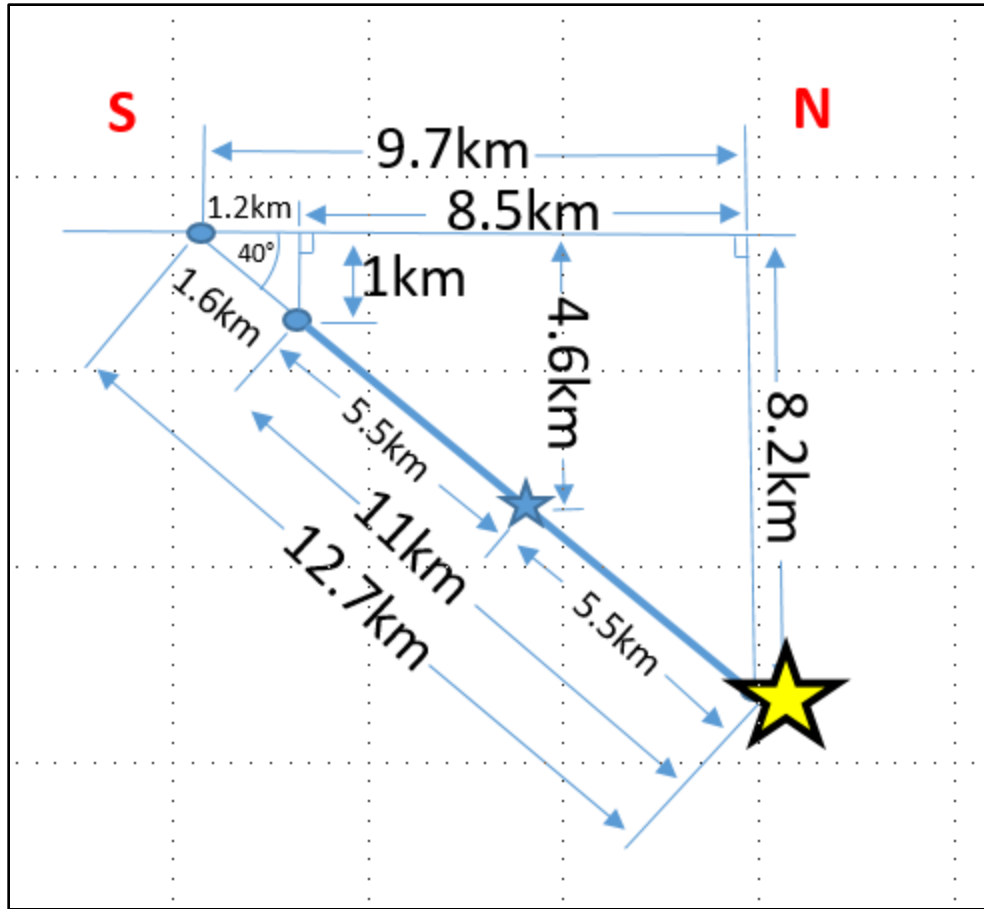
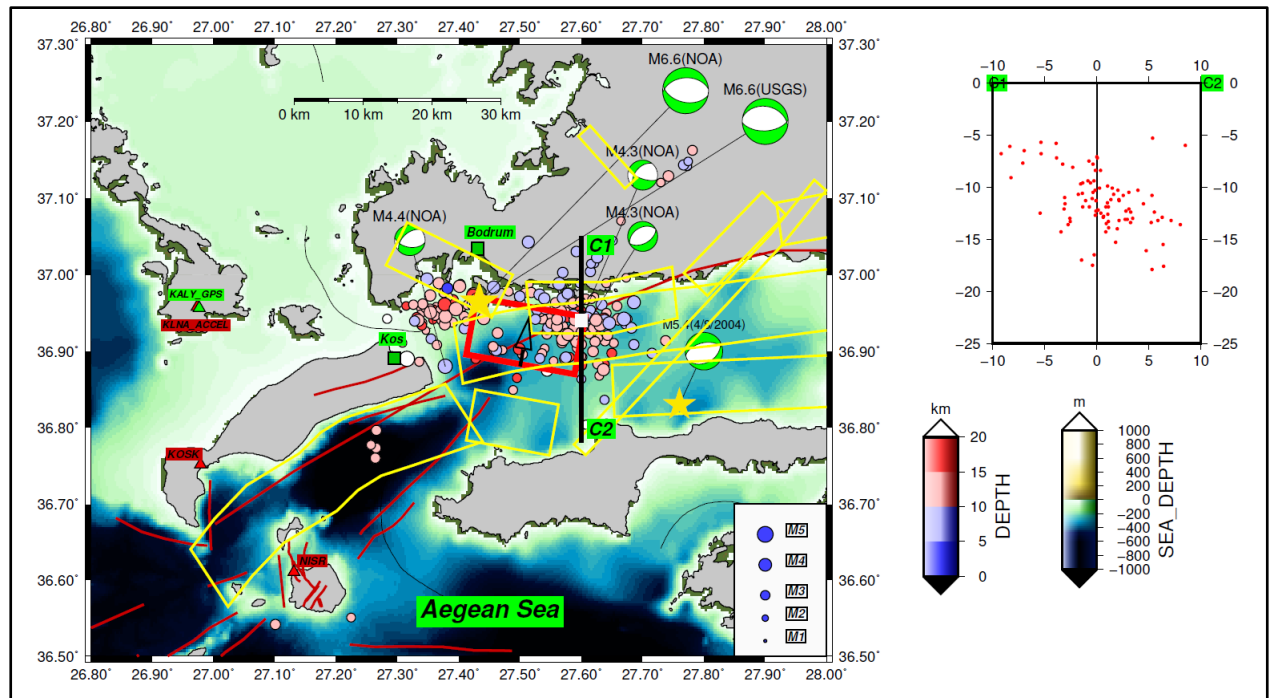


Figure 5. Schematic section across the modelled fault (for location see Fig. 3). Yellow star indicates NOA hypocentre location on this NW edge.

It is interesting to observe that most of the NOA aftershocks are located outside and around the co-seismic fault plane (Fig. 1 and Fig. 6) forming two clusters. This suggests that the main fault plane may have ruptured as in one asperity with a few unbroken patches (if any). The eastern cluster of aftershocks follows a (weakly-defined) south dipping plane (as can be seen on the N-S profile in Figure 6) that correlates with the fault source Gökova - Ören Fault Zone 3 from the SHARE database (Gürer & Yilmaz 2002, Ulug et al. 2005). The change in activated fault polarity towards the east end of the rupture indicates aftershock triggering on neighboring faults by stress transfer (we examine the static stress hypothesis below).



**Figure 6** Map of the Kos-Bodrum area showing surface projection of the offshore seismic fault (red box) that ruptured during the July 20, 2017 earthquake. Yellow polygons are SHARE seismic sources (Basili et al., 2013) and red lines are active fault traces from the NOAFaults database (Ganas et al., 2013). Beachballs represent focal mechanisms of strong earthquakes (lower hemisphere projections) reported by NOA and USGS. The 2004 focal mechanism is after Yolsal-Çevikbilen et al., (2014). Bathymetry data was provided by EMODNET. Notice the two clusters of aftershocks on either side of the seismic fault. This map was constructed on July 29, 2017 08:50 UTC.

### 3. Stress transfer modelling

Static stress changes due to the mainshock have been computed on optimally-oriented receiver faults using the Coulomb failure criterion (King et al., 1994; Toda et al., 2011), assuming source parameters listed in Table 2 and N-S regional extension. The result presented in Fig. 7 shows stress shadows across the fault and it explains well the marginally on- and mainly off-plane distribution of the aftershock distribution. Therefore, it is suggested that the aftershocks have been triggered due to static stress loading. The cross-section image across the Coulomb failure model (Fig. 8) with respect to the NOA hypocenters' distribution supports the abovementioned statement that the main fault plane ruptured as in one asperity - not leaving unbroken patches - surrounded by loaded areas where slip occurred. We also note that triggered seismicity is restricted within less-than-one fault length.

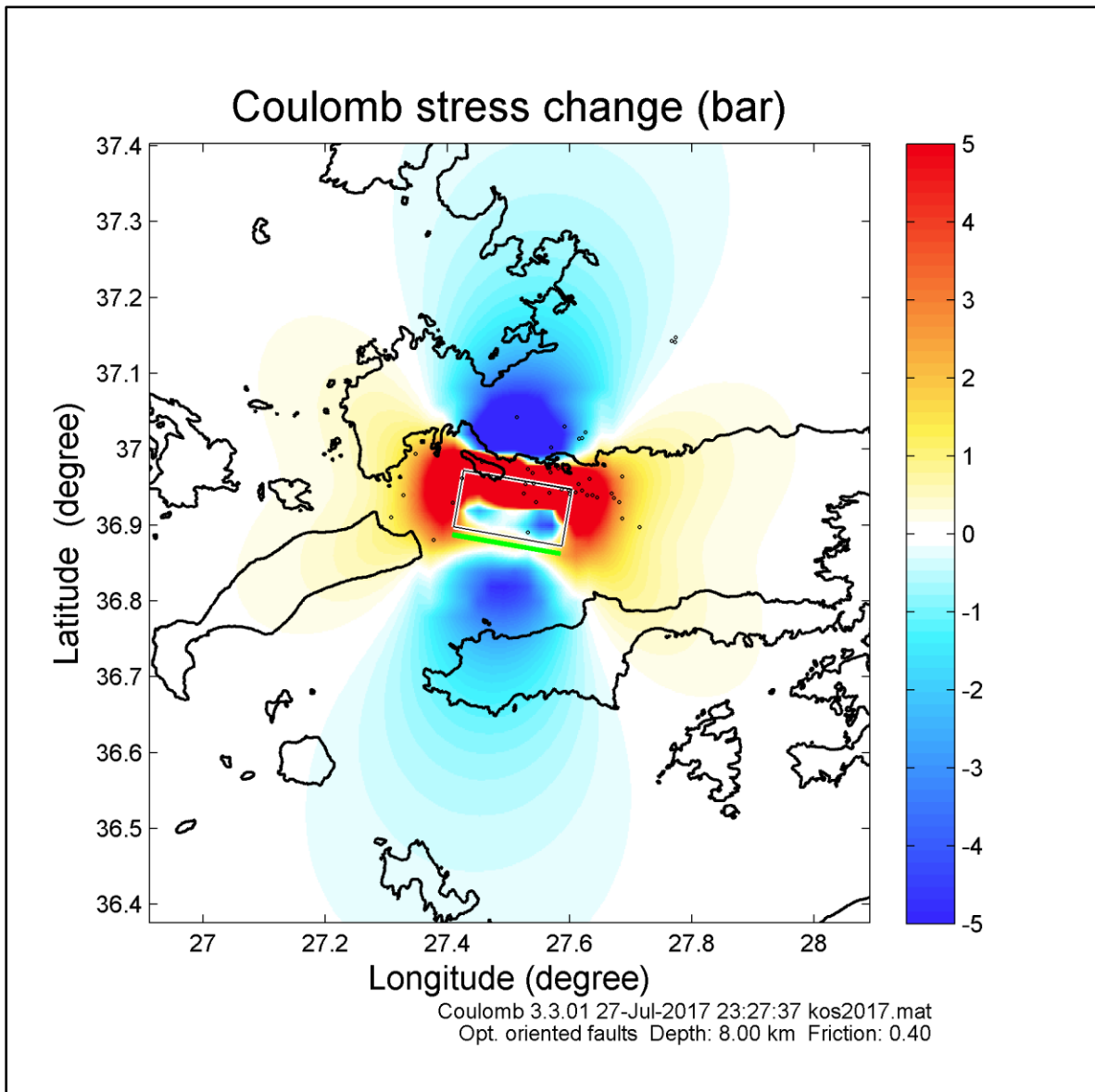


Figure 7. Coulomb stress changes at 8-km depth associated with the July 20, 2017, 22:31 UTC Mw 6.6 earthquake. The palette of Coulomb stress values is linear in the range  $-5$  to  $+5$  bar. The stress change has been computed on planes optimally oriented to regional tectonics (N-S extension). Blue areas, unloading (relaxed); red areas, loading. White rectangle is the surface projection of the ruptured plane, and green line is its surface trace. Open circles are NOA aftershocks located at  $8 \pm 1$  km depths for the period July 20-28, 2017. The source slip model is that of Figure 5. Color scale in bar (1 bar = 100 KPa).

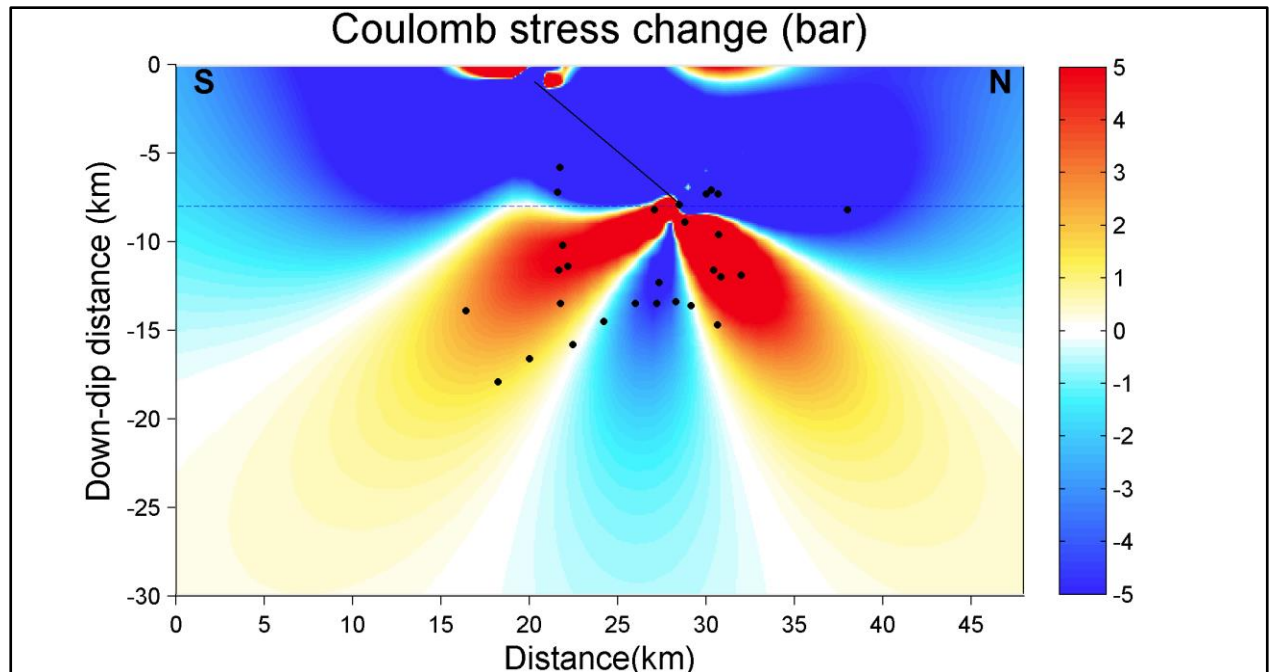


Figure 8. Vertical cross-section crossing the centroid of the July 20, 2017 event heading N190°E. Thick black line (inclined towards north) indicates seismic source. Thin horizontal line depicts the map slice of Coulomb stress (DCFF) distribution shown in Figure 7. Solid circles are NOA aftershock locations for the period 20-28 July 2017.

#### 4. Fault relation to tsunami effects

Subsidence shown near Alikarnassos (Bodrum) in differential interferometry by Harokopeion University in Athens (communicated on Jul. 25, 2017) and the National Observatory of Athens (NOA; also communicated on Jul. 25, 2017; Figure 2) appears to be in agreement with the flooding observed around Alikarnassos (Bodrum) coast from data collected during post tsunami field survey<sup>6</sup> (Dr Ahmed Yalciner, personal correspondence). The compilation of observations collected as part of the post-tsunami field survey in all nearby coastlines of Turkey affected by the tsunami, are part of a preliminary report that mentions a first negative wave motion (receding wave) also shown on the tide gauge (Figure 9). This also agrees with the fault model proposed in this report where the dip-direction of the normal fault is pointing towards Alikarnassos (Bodrum; Figure 3) which is located upon the side of the fault with the downward motion. From the same

<sup>6</sup> <http://users.metu.edu.tr/yalciner/july-21-2017-tsunami-report/Report-Field-Survey-of-tsunami-effects-at-S-of-Bodrum-Peninsula.pdf>

field survey, the largest damage on the Turkish coast from the tsunami was observed at Gumbet Bay, 3 km of Alikarnassos (Bodrum) where many boats were damaged and washed onshore. On the Greek coastline flooding was observed in the island of Kos which sustained the largest damage from both the earthquake and tsunami. Streets were flooded and also some boats were washed onshore (<http://www.newsbeast.gr/greece/arthro/2776501/mini-tsounami-stin-ko-apo-ton-sismo> ). Few eyewitness reports of inundation extent mention as much as 100 m inland but those have not been confirmed yet. Preliminary estimates indicate smaller inundation extent from the tsunami on the Greek coastlines than what was recorded on the Turkish coast ( $\leq 60\text{m}$ ).

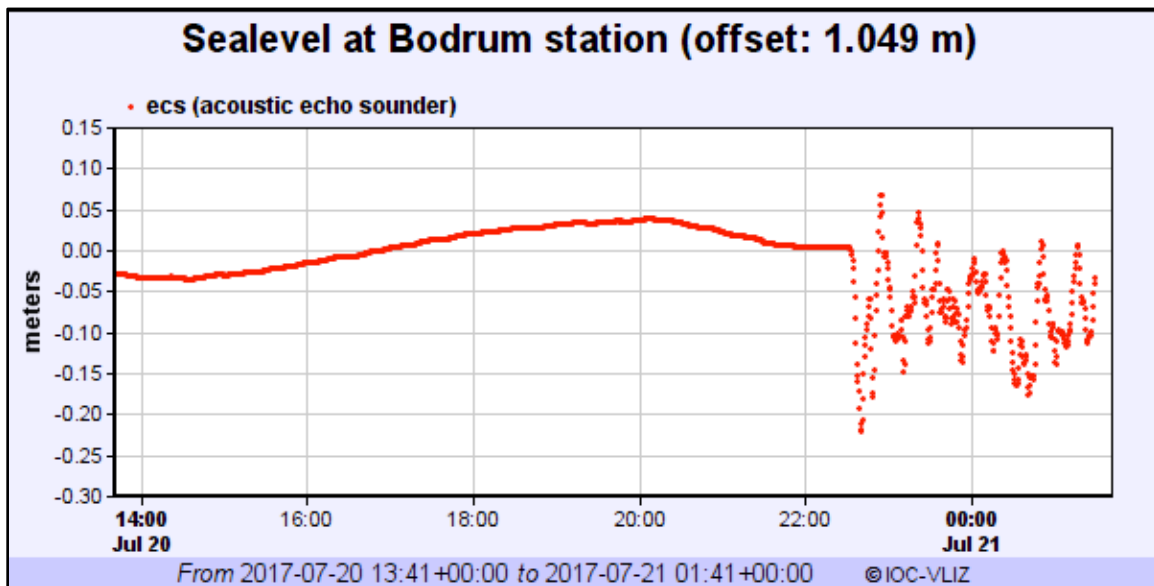


Figure 9. Tide-Gauge record of Bodrum station of IOC<sup>7</sup>.

Both recent, strong events near Lesvos (June 12, 2017; Ganas et al., 2017) and near Kos show that tsunamigenesis is likely in the Aegean basin from events that fall below 7.0 or 7.5 in magnitude, common cut-offs in magnitude for tsunami sources of tectonic origin in many hazard and risk studies (e.g. Geist and Parsons, 2005; Geist and Lynett, 2014; <http://www.air-worldwide.com/Press-Releases/AIR-Worldwide-Releases-Updated-Earthquake-Model-for-the-United-States/> ). Also, the 2017 observations confirm that the threat from tsunamis in the Aegean is real and serious damage and flooding can follow even relatively small-for tsunamigenesis-tectonic events (e.g. Papadopoulos et al., 2014).

<sup>7</sup> <http://www.ioc-sealevelmonitoring.org/station.php?code=bodr>

## 5. Aftershock statistics

We also analysed the early aftershock data plotted in Fig. 6. The NOA catalogue (revised solutions) contains 203 aftershocks with local magnitude larger than 1.7 that have been recorded within  $8\frac{1}{4}$  days after the main shock. We note (see Fig. 10) that no aftershock with  $4.8 < M < 6$  has occurred up to the time this report was compiled, as it is usually expected in aftershock sequences in the Aegean region (Drakatos and Latoussakis, 2001).

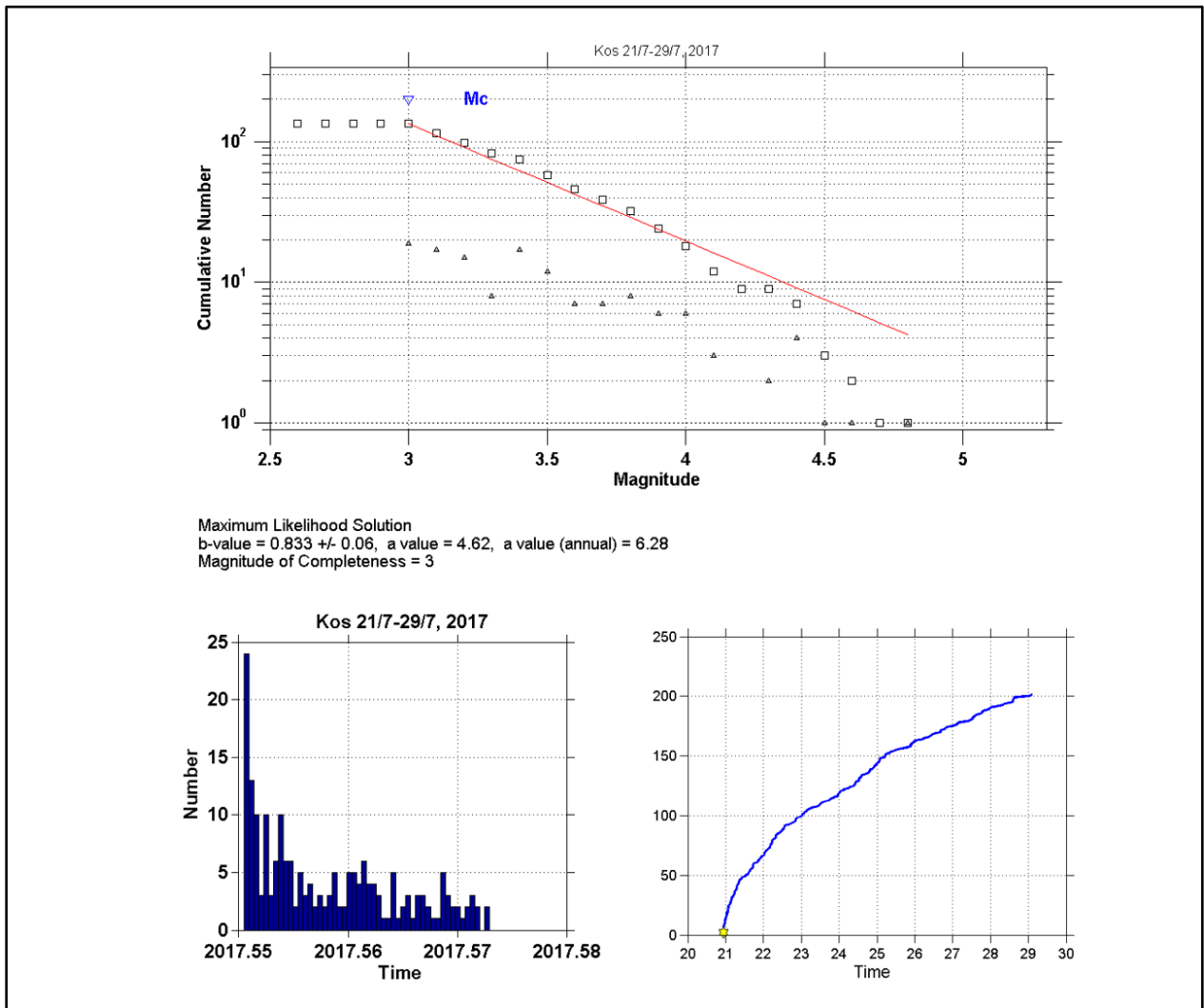


Figure 10. Early statistics of the aftershock sequence of the Kos earthquake ( $N=203$ ; NOA catalogue data as of 29 July 2017 morning): top) Magnitude–frequency distribution of aftershocks ( $b= 0.83$ ; maximum likelihood estimate, with magnitude of completeness  $M_c= 3.0$ ) lower left) time-distribution of aftershocks lower right) cumulative number of aftershocks with time. Analysis done by ZMAP software (Wiemer, 2001).

## 6. Conclusions

Our preliminary conclusions are:

- a) On 20<sup>th</sup> July of 2017 22:31 UTC a shallow  $M_w=6.6$  event occurred along an offshore normal fault east of Kos and beneath islet Karaada (south of Bodrum), SE Aegean Sea. The earthquake generated up to 20 cm surface deformation (subsidence) that was mapped by InSAR.
- b) Kinematic analysis of GNSS data (station DATC; Fig. 4) showed co-seismic offsets of about 3 cm towards South and 1 cm towards East.
- c) We modelled the seismic fault by combining the ascending and descending Sentinel observations. Mixing ascending and descending orbits provides a more robust solution. We find that we can model the overall fringe pattern by putting 1.5 m of normal slip on a north-dipping fault.
- d) The inversion of geodetic data suggests that the upper edge of the fault is offshore (near the Gokova ridge bathymetric feature; Fig. 1), and at a very shallow depth ( $1\pm 0.5$  km), as constrained by InSAR observations. The fault plane strikes  $N280^\circ E$  and dips to the north with an angle of about 40 degrees.
- e) This fault model is compatible with published seismological data (MT solutions; Table 1) and the spatial distribution of aftershocks.

## 7. Acknowledgements:

We thank the NOA seismic analysis group for the earthquake locations. Sentinel 1A images were provided free by ESA's Sentinels Scientific Data Hub. Bathymetry data were retrieved from EMODNET and topography from ALOS global model (30-m). We thank Ahmed Yalciner, Evi Nomikou, I. Parcharidis, M. Sachpazi, R. Reilinger, S. Ergintav and E. Lekkas for comments and discussions. We also thank the Greek private networks, METRICANET <http://www.metricanet.gr/> and URANUS (TREE Co, <http://www.uranus.gr/>) and the Turkish GCM network for releasing their GNSS data. Several figures were prepared by use of GMT software (Wessel et al., 2013).

## 8. References

Basili R., Kastelic V., Demircioglu M. B., Garcia Moreno D., Nemser E. S., Petricca P., Sboras S. P., Besana-Ostman G. M., Cabral J., Camelbeeck T., Caputo R., Danciu L., Domac H., Fonseca J., García-Mayordomo J., Giardini D., Glavatovic B., Gulen L., Ince Y., Pavlides S., Sesetyan K., Tarabusi G., Tiberti M. M., Utkucu M., Valensise G., Vanneste K., Vilanova S., Wössner J. 2013. The European Database of Seismogenic Faults (EDSF) compiled in the framework of the Project SHARE. <http://diss.rm.ingv.it/share-edsf/> , doi: 10.6092/INGV.IT-SHARE-EDSF.

Briole, P., De Natale, G., Gaulon, R., Pingue, F. & Scarpa, R., 1986. Inversion of geodetic data and seismicity associated with the Friuli earthquake sequence (1976-1977), *Annales Geophysicae*, 4(B4), 481-492.

Drakatos, G. and J. Latoussakis, 2001. A catalog of Aftershock Sequences in Greece (1971 – 1997) – Their Spatial and Temporal Characteristics. *Journal of Seismology*, 5, pp 137 – 145.

Floyd, M. A., et al. 2010. A new velocity field for Greece: Implications for the kinematics and dynamics of the Aegean, *J. Geophys. Res.*, 115, B10403, doi:10.1029/2009JB007040.

Ganas, A., and T. Parsons, 2009. Three-dimensional model of Hellenic Arc deformation and origin of the Cretan uplift, *J. Geophys. Res.*, 114, B06404, doi:10.1029/2008JB005599.

Ganas A., Oikonomou I.A. and Tsimi Chr, 2013. NOAfaults: a digital database for active faults in Greece. *Bulletin of the Geological Society of Greece*, vol. 47 (2), 518-530, <http://dx.doi.org/10.12681/bgsg.11079>

Ganas, A., P. Briole, P. Elias, P. Korkouli, A. Moshou, S. Valkaniotis, M. Rogier, M. Foumelis, P. Argyrakis, I. Parcharidis, 2017. Preliminary characteristics of the June 12, 2017 M6.3 Plomari earthquake sequence (Lesvos, Greece) from seismic and geodetic data, *Safe Athens 2017 Book of Abstracts*, page 16.

Geist, E. L., and T. Parsons, 2005. Probabilistic analysis of tsunami hazards, *Nat. Hazards*, 37(3), 277–314.

Geist, E. and Lynett, P., 2014. Source Process in the Probabilistic Assessment of Tsunami Hazards. *Oceanography* 27(2), pp. 86-93, doi: 10.5670/oceanog.2014.43.

Goldstein, R. & Werner, C., 1998. Radar interferogram filtering for geophysical applications, *Geophys. Res. Lett.*, 25, 4035–4038.

Gürer, Ö.F. and Yilmaz, Y. 2002. Geology of the Ören and Surrounding Areas, SW Anatolia. *Turkish J. Earth Sci.*, 11, 1-13.

Irmak S, 2013. Focal mechanisms of small-moderate earthquakes in Denizli Graben (SW Turkey). *Earth Planets Space*, 65, 943–955.

İşcan, Y., Tur, H., Gökaşan, E., 2013. Morphologic and seismic features of the Gulf of Gökova, SWAnatolia: evidence of strike-slip faulting with compression in the Aegean extensional regime. *Geo-Mar. Lett.* 33 (1), 31–48.

Kiratzi A, Louvari E, 2003. Focal mechanisms of shallow earthquakes in the Aegean Sea and the surrounding lands determined by waveform modelling: a new database. *J. Geodyn* 36(1–2):251–274

Kreemer, C., and N. Chamot-Rooke, 2004. Contemporary kinematics of the southern Aegean and the Mediterranean Ridge, *Geophys. J. Int.*, 157, 1377– 1392, doi:10.1111/j.1365-246X.2004.02270.x.

King, G.C.P., Stein, R.S., and Lin, J., 1994. Static stress changes and the triggering of earthquakes, *Bull. Seism. Soc. Am.*, 84(3), 935-953.

Nomikou, P., Papanikolaou, D., 2011. Extension of active fault zones on Nisyros volcano across the Yali-Nisyros Channel based on onshore and offshore data. *Mar. Geophys. Res.* 32 (1/2), 181–192. <http://dx.doi.org/10.1007/s11001-011-9119-z> .

Nomikou, P., Papanikolaou, D., Alexandri, M., Sakellariou, D., Rousakis, G., 2013. Submarine volcanoes along the Aegean volcanic arc. *Tectonophysics* 597–598, 123–146. <http://dx.doi.org/10.1016/j.tecto.2012.10.001>.

Papadopoulos, G., et al., 2014. Historical and pre-historical tsunamis in the Mediterranean and its connected seas: Geological signatures, generation mechanisms and coastal impacts. *Marine Geology*, 354, 81–109.

Tibaldi A., Pasquarè F.A., Papanikolaou D., Nomikou P. 2008. Tectonics of Nisyros Island, Greece, by field and offshore data, and analogue modeling. *Journal of Structural Geology*, 30(12), 1489-1506.

Toda, S., Stein, R.S., Sevilgen, V., Lin, J., 2011. Coulomb 3.3 Graphic-rich deformation and stress-change software for earthquake, tectonic, and volcano research and teaching-user guide. U.S. Geological Survey Open-File Report 2011-1060, 63, <http://pubs.usgs.gov/of/2011/1060/>

Tur, H., et al., 2015. Pliocene–Quaternary tectonic evolution of the Gulf of Gökova, southwest Turkey, *Tectonophysics*, <http://dx.doi.org/10.1016/j.tecto.2014.11.008>

Ulug, A., Duman, M., Ersoy, S., Özel, E., Mert Avci, M. 2005. Late Quaternary sea level change, sedimentation and neotectonics of the Gulf of Gökova: Southeastern Aegean Sea. *Marine Geology*, 221(1-4), 381-395, doi: 10.1016/j.margeo.2005.03.002

USGS <https://earthquake.usgs.gov/earthquakes/eventpage/us20009ynd#moment-tensor>

Vernant, P., Reilinger, R., McClusky, S., 2014. Geodetic evidence for low coupling on the Hellenic subduction plate interface. *Earth Planet. Sci. Lett.* 385 (C), 122–129. <http://dx.doi.org/10.1016/j.epsl.2013.10.018>

Wessel, P., W. H. F. Smith, R. Scharroo, J. F. Luis, and F. Wobbe, 2013, *Generic Mapping Tools: Improved version released*, *EOS Trans. AGU*, 94, 409-410.

Wiemer, S. 2001. A Software Package to Analyze Seismicity: ZMAP. *Seismological Research Letters*, Vol. 72, 373-382.

Yolsal-Çevikbilen Seda, Tuncay Taymaz, Cahit Helvacı, 2014. Earthquake mechanisms in the Gulfs of Gökova, Sığacık, Kuşadası, and the Simav Region (western Turkey): Neotectonics, seismotectonics and geodynamic implications, *Tectonophysics*, Volume 635, Pages 100-124, <http://dx.doi.org/10.1016/j.tecto.2014.05.001> .

**END OF REPORT**